Article

Modelling the Chemical Mechanism of the Thermal Atomic Layer Etch of Aluminium Oxide: A Density Functional Theory Study of Reactions During HF Exposure

Suresh Kondati Natarajan, and Simon D. Elliott

Chem. Mater., **Just Accepted Manuscript** • DOI: 10.1021/acs.chemmater.8b01930 • Publication Date (Web): 09 Aug 2018

Modelling the Chemical Mechanism of the Thermal Atomic Layer Etch of Aluminium Oxide: A Density Functional Theory Study of Reactions During HF Exposure

Suresh Kondati Natarajan † and Simon D. Elliott*,†,‡

†*Tyndall National Institute, University College Cork, Lee Maltings, Dyke Parade, Cork, T12 R5CP, Ireland.*

‡*Currently at Schrödinger Inc., 120 West 45 th Street, 17 th Floor, New York, NY 10036-4041, USA.*

E-mail: simon.elliott@schrodinger.com

Abstract

Thermal atomic layer etch, the reverse of atomic layer deposition, uses a cyclic sequence of plasma-free and solvent-free gas-surface reactions to remove ultra thin layers of material with a high degree of control. A theoretical investigation of the hydrogen fluoride pulse in the thermal atomic layer etch of monoclinic alumina has been performed using density functional theory calculations. From experiments, it has been speculated that the HF pulse forms a stable and non-volatile layer of AlF_3 on alumina surface. Consistent with this, the desorption of an AlF_3 molecule from an HF saturated surface was computed to be energetically unfavourable. HF molecules adsorbed on the alumina surface by forming hydrogen bonds, and either remained intact or dissociated

to form Al-F and O-H species. At higher coverages, a mixture of molecularly and dissociatively adsorbed HF molecules in a hydrogen-bonded network was observed. Binding energies converged as the coverage of dissociated F became saturated, consistent with a self-limiting reaction. The formation of H_2O molecules in the HF pulse was found to be endoergic with an energy barrier of at least +0.9 eV, but their subsequent desorption was computed to cost as little as +0.2 eV. Based on a model of the saturated Al-F surface, the theoretical maximum of the etch rate was estimated to be -0.57±0.02 Å/cycle (-20.0±0.8 ng/(cm^2 cycle)), which matches the range of maximum experimental values. The actual etch rate will, however, be dependent on the specific reagent used in the subsequent step of the atomic layer etch cycle.

Introduction

With Moore's law driving semiconductor devices to ever-smaller dimensions, atomic scale precision in device fabrication has become imperative. While atomic layer deposition (ALD) has already been established as a key enabler in cutting-edge semiconductor device manufacturing,[1–3] it still has to be augmented with robust atomically-controlled selective etching in order to fabricate next generation devices.[4,5] Historically, etching of materials has been performed using plasma in the process known as 'dry etching'.[6,7] The plasma, an energized gas containing ions and radicals, continuously etches the material as long as it is switched on, or until stops or masks are reached, making it a relatively uncontrolled process. Since the critical dimensions of semiconductor devices have shrunk tremendously, etch accuracy down to a single atomic layer has become necessary.

Atomic layer etch (ALE) opens up a new degree of control in material processing, as well as lowering cost by removing the need for etch stops.[8–10] In ALE, the substrate is sequentially exposed to self-limiting etch reactions that affect the substrate material just one atomic layer at a time. This can also be understood in terms of the synergy concept published by Kanarik *et. al.*[11] Currently, there are two different approaches to ALE.[4] In the

first approach, the surface is modified by halogenation and high energy ion bombardment is then used to remove the modified layer.[12–14] This method is anisotropic in nature since the energized ions travel towards the surface in one direction only. In order to keep this step as self-limiting as possible, accurate control on the ion energies and process conditions are required. An alternative approach to the use of high energy ions is termed 'thermal' ALE, as it uses thermally-activated reactions to remove the modified layer instead, for example ligand exchange reactions. Since only un-ionized gas phase precursors are used, this method allows for isotropic etching of materials even at high aspect ratios. Typically, the thermal energy used in such etch processes is much lower than the ion bombardment energy and therefore this method could be used when materials are sensitive to the high energy techniques. For particular applications a combination of directional plasma ALE and thermal ALE can also be considered.

Thermal ALE can also be viewed as the reverse of atomic layer deposition (ALD) in which the target material is grown up a fraction of an atomic layer in each cycle. In ALD, the success of the technique depends on the ability to create a stable and non-volatile layer at the surface of the substrate. Conversely, the focus in thermal ALE is in the formation of a layer of volatile species via surface reactions. Combining ALD and thermal ALE could allow the manufacture of an ultra-smooth thin film where ALD grows the film and thermal ALE smoothens it.[9] Thermal ALE is thus likely to be essential for the sub-10 nm critical dimensions in semiconductor technology, *e.g.* to process nanowires and nanosheets for gate-all-around transistors[5] and vertical NAND flash memories.

A thermal ALE cycle typically consists of two precursor pulses and two purges as shown in Fig. 1a. In the first pulse, precursor-1 is allowed to interact with the clean substrate that must be etched and chemically 'modifies' the exposed surface atomic layer. This surface modification has to be self-limiting in nature, *i.e.* the intermediates produced in the reaction must not be volatile species that would continuously desorb and lead to uncontrolled etching of the substrate. Any additional precursor molecules that do not participate in the

surface modification and other by-products are purged away efficiently. In the second pulse, precursor-2 (for example, a ligand exchanging agent) is introduced into the ALE chamber so as to interact with the modified layer of the substrate and produce stable and volatile by-products. It is important once again that this step is also self-limiting in nature and that the precursor-2 molecules do not interact with the 'un-modified' substrate atoms. The volatile by-products and un-reacted precursor molecules are then safely removed in the second purge event, which leaves a clean substrate layer. This completes one ALE cycle. In some cases, the second precursor pulse may leave non-volatile species at the surface which may block surface sites for the first precursor in the next cycle.

The thermal ALE cycle of Al_2O_3 with alternating fluorination (using HF) and ligand exchange reactions (using $Sn(acac)_2$) was developed by George & co-workers[15] and the proposed mechanism is given in Fig. 1b. In the first pulse, HF gas is introduced on a clean Al_2O_3 surface. The HF molecules adsorb on to the surface and form a stable and non-volatile "AlF_3" layer, releasing H_2O as by-product, which is purged away along with un-reacted HF. The spectral signature of an AlF_3 layer on alumina has also been identified using FTIR experiments.[16] Subsequently, a second precursor $Sn(acac)_2$ is introduced that exchanges its ligands with the AlF_3 layer and is proposed to produce volatile Sn(acac)F and $Al(acac)_3$, which are flushed away in the subsequent purge step. One ALE cycle is thus completed and has achieved etching of the Al_2O_3 surface. These two precursors are also effective in the etching of other compounds such as hafnium oxide[17] and aluminium nitride.[18] Trimethylaluminium (TMA) has also been found to be an effective precursor for the ligand exchange pulse of Al_2O_3 ALE.[19] Since TMA and HF are also used as precursors for the ALD of AlF_3 films, there will be competition between AlF_3 ALD and Al_2O_3 ALE in this case.[20,21]

In this paper, we use DFT calculations to probe the HF pulse in detail so as to understand the mechanism of fluorination of a bare θ-alumina surface. Our main goal is to identify the key step that converts the Al-O bonds in the clean alumina surface to Al-F bonds during the HF pulse. Based on that, a HF saturated surface model of ALD-deposited alumina will

be constructed and a theoretical maximum of the etch rate will be deduced.

Method and Computational Details

In this paper, bulk as well as slab (surface) calculations have been performed within density functional theory using the Vienna ab initio simulation package (VASP),[26] which uses plane wave basis sets to describe valence electrons, here with an energy cutoff of 400 eV. The calculations are performed within spin-polarized generalized gradient approximation (GGA) using the Perdew-Burke-Ernzerhof (PBE) exchange-correlation (XC) functional[27] and the behaviour of the core electrons is described by projector augmented wave (PAW) potentials.[28,29] For computing the energy of possible reactions, gas phase calculations of reagent molecules and by-products have also been performed in a large periodic box of dimension (15.0 Å× 16.0 Å× 15.5 Å) with an energy cutoff of 400 eV.

As-deposited alumina films from ALD are in general amorphous. However, the majority of theoretical studies on alumina ALD in the literature use the α phase in periodic models because it is the most stable crystalline phase. For example, first principles simulation of ALD of alumina on the α-Al_2O_3(0 0 0 1) surface has been published.[30] The mechanism of HF adsorption on the α-Al_2O_3(0 0 0 1) surface has been studied in detail by Quan *et. al.*[24] However, ALD-deposited alumina is found to transform under annealing into θ-Al_2O_3,[31] which is the most stable transition phase of alumina. We therefore use θ-Al_2O_3 as a periodic model for ALD-grown alumina in this study. The first reported ab initio investigation on the properties of bulk and surface θ-Al_2O_3 used Hartree-Fock theory.[32] In 2002, Cai *et. al*[33] studied the transformation of γ-Al_2O_3 to θ-Al_2O_3 using density functional theory (DFT) calculations. Nørskov and co-workers[34] investigated the change of surface energy with increasing thickness of θ-Al_2O_3 surface slabs using DFT calculations and reported that hydroxylated θ-Al_2O_3 surfaces may be more stable than those of α-alumina. However, we did not find any published literature on the mechanism of HF adsorption on θ-Al_2O_3 surfaces.

The unit cell of monoclinic θ-Al_2O_3 consists of 8 Al atoms and 12 O atoms with the lattice parameters, $a \neq b \neq c$ and $(\alpha = \beta) \neq \gamma$. To compute these parameters, we have simultaneously relaxed the atomic positions, cell shape and cell volume with a higher energy cutoff (550 eV) and a 2×4×4 Monkhorst-Pack K-point sampling mesh. A convergence test for the choice of K-point mesh is also performed and the results can be seen in supporting information (S1). The computed lattice parameters are compared with the experimental values[35] in Table 1 and it can be seen that there is a good agreement between them within an error of only 2%. The band gap of bulk θ-Al_2O_3 is computed to be 5 eV. The overall band structure and the contributions of Al and O to the total density of states are given in the supporting information (S2). An illustration of the equilibrium bulk geometry of θ-Al_2O_3 along the 'ac' plane is given in Fig. 2(a). Out of the 8 Al atoms per cell, 4 are located in tetrahedral coordination sites (labelled in the figure) and the other 4 in octahedral coordination sites relative to the oxygen lattice. In the equilibrium geometry, the valence electrons are found to be localized mainly around the O atoms reflecting the predominantly ionic character of Al-O bond. We also performed Bader analysis[36] on the charge density to find the valence charge on individual atoms, which revealed that only 4.6% of total valence electrons are around Al atoms (average charge = +2.43) and 95.4% are around O atoms (average charge = -1.62). We have also included the lattice constants obtained by adding dispersion corrections to the energy based on the Tkatchenko-Scheffler method[37] and from Table 1, it is evident that this additional description of dispersion does not have a substantial effect on the structure of bulk alumina.

The surface of monoclinic θ-Al_2O_3 oriented at the ($\bar{2}$ 0 1) plane is considered for the slab calculations. Even though this is not the most stable surface of θ-Al_2O_3,[34] it is considered in this study mainly because the ALD-deposited alumina has been found to grow along the ($\bar{2}$ 0 1) surface orientation.[31] A (1×4) supercell of a 13 Å thick ($\bar{2}$ 0 1) slab of θ-Al_2O_3 with fixed atoms at the bottom face and 16 Å of vacuum separating the slabs is used as the surface model ($Al_{96}O_{144}$ per cell). Calculations to obtain converged values of the K-point mesh, plane

wave energy cutoff and the vacuum thickness between slabs have been performed and the results are tabulated in the supporting information (S1). Figure. 2(b) shows the optimized geometry of the Al_2O_3 ($\bar{2}$ 0 1) slab along with the electronic valence charge density. Similar to the bulk case, it can be seen that the valence electrons are concentrated mostly around the oxygen atoms. The surface energy of the fully relaxed surface slab is found to be 7.25 eV/nm^2.

The first step of the alumina ALE process is the introduction of a fluorinating agent, in this case the HF molecule. At the optimized surface slab, HF molecules are introduced at various surface sites and at various coverages. The resulting geometries of slab and adsorbate atoms are further relaxed to obtain energetic minima. This is done in order to find the maximum possible coverage of F atoms on the alumina surface, from which then we can estimate the maximum possible etch rate. For the geometry relaxation problem we have adopted a two step approach where an estimated local minimum is first obtained from the conjugate gradient (CG) method, which is known to be efficient when the starting geometry is far from a local minimum, and the resulting geometry is re-optimized with a RMM-DIIS algorithm, which is known to be efficient close to the minimum, as implemented in VASP. The methodology of computing adsorption/binding energies and charge density difference is provided in supporting information (S3).

Results

In the first part of the results section we evaluate the energetics of several postulated reactions in order to obtain a qualitative idea of the nature of the HF pulse, whether it etches or self-limits. Following that, the mechanism of monomeric HF adsorption on a bare alumina surface is reported. This includes the estimation of minimum energy pathways for the migration of a H atom on the surface along with corresponding energetic barriers. In the next part, multiple HF adsorption and the resulting minimum energy geometries are investigated so

as to understand the saturation of the alumina surface with HF. Towards the end of this section, a possible hydrogen transport mechanism and pathways leading to the formation and desorption of water molecules is reported.

Energetics of Overall Reactions

In this section, model reactions representing the HF pulse will be postulated and their energetics will be evaluated. The reaction energies (ΔE) of the balanced reactions are listed in Table 2. Two types of reactions are considered, bulk $\longrightarrow$ gas & surf $\longrightarrow$ surf. In the case of bulk $\longrightarrow$ gas reactions, we assume bulk θ-Al_2O_3 and gaseous HF as the reactants that produce gaseous by-products. These represent continuous etch reactions that produce volatile gaseous species, restore the initial surface and thus etch away units of bulk alumina. For this computation, the equilibrium energy of bulk θ-Al_2O_3 and optimized gas phase energies of molecules are used. For the surf $\longrightarrow$ surf reactions, we assume a clean $Al_2O_3(\bar{2}\ 0\ 1)$ slab and gaseous HF as reactants and the corresponding F covered alumina surface and H_2O as products. This represents a self-limiting reaction that saturates the surface with a stable and non-volatile fluorinated layer AlF_x (not necessarily a layer of AlF_3). To model an F covered alumina surface we have introduced 18 F atoms as HF and removed 9 O atoms as H_2O from the bare alumina surface model described in the method section.

We consider three bulk $\longrightarrow$ gas reactions namely, R_1, R_2 and R_3 where AlF_3, Al_2F_6 and AlOF respectively are the gas-phase reaction by-products along with H_2O.

$$R_1 : Al_2O_{3(b)} + 6\,HF_{(g)} \longrightarrow 2\,AlF_{3(g)} + 3\,H_2O_{(g)} \quad (1)$$

$$R_2 : Al_2O_{3(b)} + 6\,HF_{(g)} \longrightarrow Al_2F_{6(g)} + 3\,H_2O_{(g)} \quad (2)$$

$$R_3 : Al_2O_{3(b)} + 2\,HF_{(g)} \longrightarrow 2\,AlOF_{(g)} + H_2O_{(g)} \quad (3)$$

These reactions are non-redox type as Al, O , H and F atoms retain their formal oxidation

states of +3, -2, +1 and -1, respectively. According to the ΔE values in Table 2, R_1 and R_3 were found to be endoergic, whereas R_2 is exoergic. Moreover, the surf $\longrightarrow$ surf reaction

$$R_4 : 3\,Al_2O_{3(surf)} + 18\,HF_{(g)} \longrightarrow 6\,AlF_{3(surf)} + 9\,H_2O_{(g)}, \quad (4)$$

is found to be exoergic with a ΔE value of -3.6 eV/Al_2O_3 which is much lower than that of R_2. We have also computed the ΔE values of the bulk $\longrightarrow$ gas reactions using the much more computationally expensive PBE0 hybrid functional and compared them to the PBE values in Table 2. It can be seen that the values obtained with the two functionals agree to within 0.04 eV/HF for R1 and R2, suggesting that the PBE functional is reliable enough for these calculations. From these simplified model it appears that HF will saturate to form an AlF_x layer and not etch away θ-Al_2O_3 by itself under reactor conditions. Therefore, the next step is to find the key mechanism responsible for this AlF_x layer formation on the alumina surface.

Adsorption of 1 HF onto Bare Alumina Surface

We initiated DFT based adsorption calculations by introducing one HF molecule to the optimized (1×4) supercell of the θ-$Al_2O_3(\bar{2}01)$ surface. Detailed geometry of this supercell is provided in the supporting information (S4). Depending on the binding site of the HF molecule, it could either adsorb molecularly or dissociatively as shown in Fig. 3. Molecular adsorption of the HF molecule to the surface via hydrogen bonding resulted in a binding energy of -0.44 eV in the geometry M^1_A. Here, M^X_Y refers to a minimum geometry with X the number of HF molecules adsorbed on the (1×4) supercell of the θ-$Al_2O_3(\bar{2}01)$ surface and the alphabetical index Y referring to a specific minimum of that configuration. For example, M^1 refers to all the possible minimum geometries of the studied alumina surface with 1 adsorbed HF molecule. When more than one minimum are considered for discussion, we refer to them as M^1_A, M^1_B and so on (see supporting information (S5)). We find that molecular adsorption

results when the F atom in HF is not close enough to a surface Al atom for binding, which could drive HF dissociation. This shows that the Al-F bonding is crucial for the HF splitting reaction to take place. In geometry M_B^1, the HF adsorbs dissociatively with a binding energy of -1.74 eV and forms -Al-F and -O-H species on the surface. A detailed analysis of the nature of the HF splitting reaction for the formation of M_B^1 is discussed further below.

Starting from M_B^1, two other minima are possible depending on where the H atom hops and binds. A further low energy minimum M_D^1 with a binding energy of -2.11 eV is possible when the H atom displaces to the adjacent row of O atoms. Alternatively when the H atom is displaced in the same row of O atoms (M_C^1), binding becomes weaker and the binding energy drops to -1.31 eV. M_D^1 and M_C^1 did not result directly from our geometry relaxation calculations, so there must be energetic barriers separating them from M_B^1. Using the climbing image nudged elastic band (CI-NEB) approach[22,23] with three images in between the minima, we computed minimum energy pathways (MEPs) connecting them and the activation energies, as shown in Fig. 4. The MEP connecting M_B^1 and M_C^1 involves hopping of the H atom to the adjacent row of O atoms first (forming M_D^1) and then hopping back. Therefore, the MEP connecting M_D^1 and M_C^1 is also calculated. The H transport MEPs M_B^1 - M_D^1 and M_D^1 - M_C^1 are shown in Fig. 4(a) and (b), respectively, with a series of superimposed H atoms representing the images connecting them. The plot in Fig. 4(c) shows the relative energy difference of the images with respect to M_B^1, from which the forward and reverse barriers connecting M_B^1 and M_D^1 are found to be +0.83 eV and +1.20 eV, respectively. Similarly, the forward and reverse barriers connecting M_D^1 and M_C^1 are computed as +1.4 eV and +0.63 eV, respectively. Therefore, the most probable pathways for H transport are from M_B^1 and M_C^1 to M_D^1.

Fig. 5 describes in detail the mechanisms involved in the dissociative adsorption of a HF molecule on $Al_2O_3(\bar{2}01)$ surface corresponding to geometry M_B^1. This figure also includes a complementary graph showing the energy change relative to the initial geometry as well as the change of inter-atomic distances between H-F, Al-F and O-H (d_{H-F}, d_{Al-F}, d_{O-H}) during

the geometry optimization. The labelled vertical dashed lines in the graph correspond to the geometries shown in the figure. Geometry (a) refers to the initial state where the HF molecule is introduced at about 3 Å from the surface. During optimization, the HF molecule approaches the surface until a hydrogen bond ($d_{O-H} < 2.5$ Å) is made with a surface oxygen atom as shown in geometry (b). In the graph, this can be observed from the correlated decrease in d_{Al-F} and d_{O-H} which ends at (b), beyond which the hydrogen bond continues to strengthen as indicated by continued decrease in d_{O-H}. Moreover, a surface Al atom is attracted by the F atom, which is evident from its out-of-lattice position and decreasing d_{Al-F}. The strengthening of the hydrogen bond and the Al-F bond leads to cleavage of the HF bond as seen in geometry (c) ($d_{H-F} > 1.2$ Å), which marks the crossover point of d_{O-H} and d_{H-F}. The favourable nature of HF bond dissociation in these circumstances is also indicated by a sharp decrease in the relative energy difference and increase in d_{H-F} beyond (c) in the graph. The splitting of HF results in the formation of isolated -Al-F and -O-H species on the surface as seen in geometry (d), which further decreases the energy difference. Beyond this point d_{Al-F}, d_{H-F}, d_{O-H} and the relative energy difference converge to stable values, indicating the formation of stable -Al-F and -O-H species resulting in the minimum geometry (e) (M_B^1 in Fig. 3). The final bond lengths of Al-F and O-H are 1.67 Å and 0.99 Å, respectively and the F bound Al atom is displaced about 1 Å upwards from its lattice position along the surface normal direction. The above-described mechanism drives the conversion of Al-O bonds into Al-F bonds by means of the HF splitting reaction, which results in the formation of an AlF_x layer at the end of the HF pulse. We find that the inclusion of dispersion corrections based on the TS scheme did not result in a significant difference in the geometry or in the binding energy values.

To identify the nature of the surface-HF bonding in M_B^1, a charge density difference plot is constructed as shown in Fig. 6 in which electrons accumulate in the yellow region and deplete in the cyan region. The charge density difference is obtained by subtracting the individual charge densities of the substrate ($\rho(Al_2O_3)$) and adsorbate molecule ($\rho(HF)$) from the charge

density of the combined geometry ($\rho(Al_2O_3 + HF)$). From the figure it can be seen that the electronegative F atom gains electrons which are polarized toward the bound Al atom at the surface and that the H atom forms a covalent bond with a surface oxygen atom (d_{O-H} = 0.99 Å). The optimized geometry and charge density difference plots are similar to those of 1 HF adsorbed on α-$Al_2O_3(0001)$ surface reported by Quan et.al.[24] We also performed Bader charge analysis and found that the surface O-H and Al-F have a charge of -0.85 and +1.62, respectively. More information on this is given in the supporting information (S6).

Adsorption of Multiple HF onto Bare Alumina

In subsequent simulations, we introduced multiple HF molecules onto the bare $Al_2O_3(\bar{2}01)$ surface with coverages ranging from 1.2 to 15.4 HF/nm^2. From the previous section we know that Al-F bond formation drives the HF splitting reaction. There are 8 topmost Al atoms on the surface of the (1x4) supercell (geometry in Fig. 2 and also in the supporting information (S4)) that can potentially form Al-F bonds readily. It is to be noted that for up to 16 HF molecules, there is a possibility that all the adsorbed HF molecules will dissociate provided they adsorb in certain fashion (see M^2_A, M^8_A and M^{16} in Fig. 7). Therefore, we introduced the HF molecules by hand in such a way that not all of the the HF would bind to those 8 Al atoms and then optimized the resulting geometries. A mixture of molecular and dissociative adsorption of HF molecules is observed in the optimized geometries shown in Fig. 7. A list of these minima along with the HF coverage, Al-F coverage and corresponding binding energies is given in Table 3. The least binding per HF is observed in the geometry with 5 HF molecules where only one HF molecule dissociated. Also comparing the binding energies of M^2_A and M^2_B geometries, it may appear that the dissociation of HF molecules would lead to lower binding energies. However, from M^8_A and M^8_B geometries it seems that the dissociation of all HF molecules is less favourable than a mixture of dissociative and molecular adsorption. In fact the greatest binding energy per HF molecule is observed in the case of M^8_B where only 4 of the adsorbed HF molecules dissociated while the others formed

hydrogen bonds with the remaining HF molecules and dissociated F atoms. Therefore, as the HF coverage increases we can expect more formation of a hydrogen bonded HF network. The transport of H atoms within this network would likely play a major role in facilitating diffusion of H to reactive O and thus the formation of a stable AlF_x layer on the alumina surface.

Scatter plots of HF coverage vs Al-F coverage, HF coverage vs binding energy and Al-F coverage vs binding energy of the minima are shown in panels (a), (b) and (c) of Fig. 8, respectively. The data points with square markers along the regression line in panel (a) correspond to minima M_A^2, M_A^8, M^{16} and M_B^{24}, where nearly all of the adsorbed HF molecules are dissociated to form Al-F bonds. The rest of the data points are below the regression line indicating that some HF molecules remain undissociated. It is evident from panel (b) that binding to the surface becomes stronger as the surface is exposed to more HF, though some levelling-off is evident at high coverages. However, in panel (c) we observe that complete dissociation of HF into Al-F is not necessary to attain the greatest binding energies. The saturating coverage of dissociated F atoms is obtained when there is a convergence in the values of binding energy in eV/nm^2. The circular markers show dissociated Al-F coverage saturating at 5-7/nm^2, with further energetic stabilization to at most -16 eV/nm^2 coming from additional molecular HF at constant Al-F. Comparing squares and circles shows that negligible energy is gained through further dissociation.

These data suggest that a coverage of 7.1±0.3 F/nm^2 of dissociated F can be readily achieved. Further molecular HF can bind and dissociate, but without lowering the surface energy appreciably. This value for the saturating F coverage will therefore be used further below to derive the etch rate. Moreover in this (1x4) supercell of θ-alumina with a surface area of 1.68 nm^2, there are 8 topmost Al atoms at the surface (see supporting information (S5)) that could readily form Al-F bonds, which corresponds to a coverage of 4.8 Al/nm^2. Therefore, for a coverage of 7.1±0.3 F/nm^2 there will be about 1.5 F atoms per surface Al atom on average.

Hydrogen Transport Mechanism

We now describe in detail the hydrogen transport mechanism observed in the adsorption of 2 HF per cell on the ($\bar{2}$01) surface of alumina, corresponding to the minimum M_C^2 in Fig. 7. The initial geometry considered for this optimization problem is shown in Fig. 9(a), where the two HF molecules are hydrogen bonded to surface oxygen atoms. Upon optimization, we have observed dissociative adsorption of only one HF molecule while the other is intact and forms hydrogen bonds with the surface -Al-F and -O-H species as shown in geometry (e) (M_C^2 in Fig. 7). The binding at this geometry shows an energy of -1.4 eV per HF, which is just 0.1 eV weaker than that of geometry M_A^2, where both HF molecules are dissociated.

The mechanism of HF dissociation observed here is different from that of the 1 HF case detailed earlier (see Fig. 5), as here the dissociated H atom did not covalently bind to the surface O atom to which it was initially hydrogen bonded, but rather to the O atom in the adjacent row. We have already seen in the case of 1 HF adsorption that H displacement to adjacent row of O atoms is energetically favourable. Fig. 9 also includes a reference graph showing the change of energy (relative to the initial geometry) and important bond distances as a function of the optimization steps. Going from (a) to (b), the initial hydrogen bond between molecule H1F1 and the surface is broken and a new hydrogen bond is beginning to form between H1F1 and H2F2. At the same time, the strengthening of bond between Al' and F1 is evident from the out-of-lattice position of Al' and the decrease in $d_{Al'-F1}$. These events lead to a decrease in the relative energy of about -0.6 eV. In the next segment, between (b) and (c), the hydrogen bond between H1F1 and H2F2 becomes stronger as evident from considerable decrease in d_{H1-F2}. Moreover, the H2F2 molecule switches its surface hydrogen bond acceptor (to O') as it is displaced closer to the H1F1 molecule due to stronger Al'-F1 binding. Towards end of the region between (c) and (d) four simultaneous events take place which lead to the transfer of H atoms:

- Dissociation of H1F1

- Dissociation of H2F2
- Formation of H1F2
- Formation of surface O'H2 species

From (c) to (d), the energy decreases gradually, but goes down steeply after the crossover point at (d) as the newly-formed surface O'H2 and H1F2 molecule stabilize. These events could be more pronounced at higher coverages where a network of hydrogen bonded HF molecules, which transfers H atoms in this fashion, could affect surface fluorination and thus influence etch rates.

H_2O Formation and Desorption

In the postulated reactions given earlier, we have assumed the release of volatile H_2O in the HF pulse. However, we did not observe any spontaneous formation and desorption of water molecules in our geometry relaxation calculations. Therefore, it will be interesting to estimate the energetic barriers involved. In Fig. 10, two pathways leading to the formation and desorption of H_2O molecules are identified using minimum geometry G1 (M_A^2 in Fig. 7) as the starting point. In the H_2O formation process, the first step is the hop transfer of one H atom to the adjacent row of O atoms (G1 $\longrightarrow$ G2). This is an exoergic event since the resulting minimum G2 is 0.14 eV lower in energy than G1. However, there is an energetic barrier of +0.92 eV to go from G1 to G2. The activation barriers discussed here are computed using CI-NEB method and the results are listed in Table 4. Since the minimum G2 is lower in energy than G1, the reverse hop of the H atom will have a slightly larger barrier of +1.06 eV.

From this point there are two possibilities for H_2O formation. The first possibility (G2 $\longrightarrow$ G3) is when the displaced H atom hops back to the OH in the initial row, crossing an energy barrier of +1.63 eV, resulting in H_2O formation. The second possibility (G2 $\longrightarrow$ G4) is when the un-displaced H atom in minimum G2 also hops to the OH in adjacent row

and forms H_2O after crossing an energy barrier of +1.79 eV. In both cases the resulting geometries G3 and G4 are higher in energy than G2 by 1.21 eV and 1.44 eV, respectively. Therefore, the formation of H_2O is endoergic at T=0 K and is dependent on the ALE operating conditions (T and p). The reverse pathways G3 $\longrightarrow$ G2 and G4 $\longrightarrow$ G2 have relatively lower barriers of +0.19 eV and +0.58 eV, respectively. Therefore, the water molecules must desorb before they disintegrate and reform minimum G2 once again. The desorption energies of the H_2O from geometries G3 and G4 are computed to be +0.26 eV and +1.17 eV, respectively (corresponding to minima G5 and G6). Based on the above results for the two pathways, G1-G2-G3-G5 and G1-G2-G4-G6, the former seems more preferable due to the relatively lower activation energies for H_2O formation and desorption.

If H_2O molecules are not formed and OH persists at the alumina surface, this is likely to lead to TMA adsorption via the competing surface reaction

$$\mathrm{OH_{(surf)}} + \mathrm{Al(CH_3)_{3(gas)}} \longrightarrow \mathrm{O{-}Al(CH_3)_{2(surf)}} + \mathrm{CH_{4(gas)}}. \quad (5)$$

Moreover, as already mentioned, the same precursors HF and TMA are used in the ALD of AlF_3[20,21] which might lead to a competition between the ALE of Al_2O_3 and the ALD of AlF_3. On the other hand, if $Sn(acac)_2$ is used as the second precursor, the persistent surface OH species might also lead to $Sn(acac)_2$ adsorption via the following reaction

$$\mathrm{OH_{(surf)}} + \mathrm{Sn(acac)_{2(gas)}} \longrightarrow \mathrm{O{-}Sn(acac)_{(surf)}} + \mathrm{acacH_{(gas)}}. \quad (6)$$

Discussion

We started our investigation of the HF pulse on alumina by comparing the reaction energies of continuous bulk etching and those of surface saturation. In both cases, it is assumed that the surface oxygen atoms are removed as H_2O molecules. We found that the saturating surface reaction was energetically more favourable than the continuous etching reactions by

at least 2 eV/Al_2O_3. This suggested that the HF pulse is self-limiting in nature, forming a stable and non-volatile AlF_x layer on the alumina surface.

As the next step, we studied the adsorption mechanism of 1 HF molecule per cell on the model θ-Al_2O_3 surface in order to identify the key reaction step responsible for the conversion of Al-O bonds in the surface to Al-F bonds. With a computed dipole moment of 1.8 Debye, the HF molecule initially physisorbed to the bare alumina surface by means of strong dipole interactions. We observed that the HF molecule can next chemisorb either molecularly or dissociatively. In either case, the HF molecule initially formed an hydrogen bond with a surface O atom. Based on whether the F atom was oriented so as to find an Al partner on the surface or not, the HF molecule either remained intact or dissociated to form surface-bound Al-F and O-H species. The HF bond is strong with a bond dissociation energy of 6 eV. On adsorbing to the alumina surface, the HF bond did not begin to dissociate until the O-H and Al-F bonds are almost formed (evident from the bond distances in Fig. 5). The splitting of the HF bond correlates closely with the reduction of the total energy of the system. In the case of dissociative adsorption, we found that the adsorbed H atom could hop to other atop O sites on the surface subject to energetic barriers. The hop of H to an adjacent row of O atoms away from the Al-F was energetically preferred, albeit impeded by a barrier of +0.83 eV. It cost energy for H to hop to an adjacent O atom in the same row.

As the coverage of HF was increased in our simulations, we observed a mixture of intact and dissociated HF molecules that formed a hydrogen bonded network on the surface. In fact, such a mixed adsorption state was found to be similar in energy to the state where almost all HF molecules were dissociated. This indicates that after the initial surface coating of AlF_x, there is little energetic driving force for further dissociation of HF molecules, potentially therefore achieving the self-limiting condition. No spontaneous formation of the discrete AlF_3 molecule is observed at the surface in our calculations even at high HF coverages. Moreover at the saturating dissociated F coverage of 7.1$\pm$0.3 F/nm^2, we find that on average only 1.5 F atoms are bound to each surface Al atoms. Our investigations further indicate that

such a molecule (AlF_3) would be involatile, as evidenced by a very high computed energy of +2.75 eV at T=0 K for desorption from the HF-saturated surface M_B^{24} in Fig. 7. Similarly, the desorption energy of the Al_2F_6 molecule is found to be +3.17 eV. Exposing the surface to various coverages of HF, we observe saturation in the coverage of dissociated F (at 5-7 F/nm^2) and eventually also saturation in the binding energy (at -16 eV/nm^2) even when additional HF molecules are present. Taken together, these findings strongly suggest that the HF reaction is self-limiting, which is a key requirement for thermal ALE. To confirm this will require detailed study of diffusion pathways of F into Al_2O_3 sublayers, including relaxation of associated stress in large simulation cells.

The un-reacted HF molecules as well as any H_2O formed should be removed in the purge step, leaving an AlF_x covered alumina surface. The desorption energies of AlF_3 and Al_2F_6 relative to the AlF_x layer on alumina surface obtained after the purge are computed to be as high as +5.08 eV and +5.24 eV, respectively, substantially higher than the desorption energies quoted above. Evidently, the molecules bind more strongly to the surface when some surface O atoms have been removed as H_2O. The geometries used for the above calculations are shown in the supporting information (S7).

Since the HF reaction self-limits, a co-reagent is needed to chemically remove residual F and Al atoms from the surface and complete the ALE cycle. In the literature, $Sn(acac)_2$[15] and $Al(CH_3)_3$[10] have been demonstrated to be successful co-reagents. Analysis of the ligand exchange mechanisms between the AlF_x layer and the above mentioned co-reagents is beyond the scope of this paper.

Having established the chemical nature of the saturating surface in one of the ALE pulses, we are now able to estimate the maximum etch rate that is theoretically possible. Of all the AlF_x covered surface models that we computed, it can be seen from the Al-F coverage and surface energy values in Table 3 that M^{26} (Fig. 7) is the most probable representative geometry of the saturated surface. Although M_B^{24} is slightly more stable at T=0 K, M^{26} has a similar binding energy per unit area at considerably lower Al-F coverage. The coverage

of dissociated F in M[26] is 7.1±0.3 F/nm^2. The maximum etch rate can clearly be achieved when all of this dissociated F leads to etching of Al_2O_3 in each ALE cycle. According to the etch reactions proposed by George and co-workers,[15,16,19] three F atoms lead to the etching of one Al atom, and so the coverage of Al that can be etched is one third of the F coverage, 2.4±0.1 Al/(nm^2 cycle). Since the surface layer of θ-$Al_2O_3(\bar{2}01)$ shows an Al coverage of 4.8±0.3 Al/nm^2, this maximum etch rate corresponds to 0.5 monolayer/cycle. Converting to other units, this etch rate is -20.0±0.8 ng/(cm^2 cycle) and, via the mass density of bulk θ-alumina (3.5 g/cm^3), -0.57±0.02 Å/cycle. (For the sake of comparison, the removal of a complete monolayer of Al_2O_3 would require a dissociated F coverage of 14.2±0.3 F/nm^2 and the corresponding etch rate would be -1.14±0.02 Å/cycle or -40.0±0.8 ng/(cm^2 cycle)). Clearly, the etch rate will be lower in magnitude than the theoretical maximum of 0.57±0.02 Å/cycle if reaction kinetics do not allow the etch reaction to proceed to completion. This could happen if residual F remains adsorbed at the surface after the ligand exchange pulse or if the desorption of H_2O is incomplete. Indeed, residual OH at the surface could allow competing ALD growth reactions to take place when TMA is used as the ligand exchange reagent.[20,21]

Using HF and $Sn(acac)_2$ as precursors, George and co-workers[15] report etch rates ranging from -4.1 ng/(cm^2 cycle) at 150°C to -18.3 ng/(cm^2 cycle) at 250°C from quartz crystal microbalance measurements, albeit hindered by residual acac impurities. The higher temperature value is very close to our predicted maximum of -20.0±0.8 ng/(cm^2 cycle). An additional H_2 plasma pulse after the $Sn(acac)_2$ pulse has been reported to increase the etch rates from 0.36 to 1.96 Å/cycle in the case of aluminium nitride using the same precursors.[18] This additional plasma pulse seems to remove the acac residual impurities on the surface after the ligand-exchange pulse. Therefore, the etch rates of alumina can perhaps also be improved by similar means. Alternatively, when trimethylaluminium (TMA) is used for the ligand exchange pulse the experimental etch rate varies from -4.2 ng/(cm^2 cycle) at 250°C to -23.3 ng/(cm^2 cycle) at 325°C.[19] The upper value is slightly higher than the maximum

rate that we predict. It appears therefore that the ligand exchange precursor also has an effect on the actual etch rate and temperature behavior.

We can speculate that the hydrogen bonded network of HF molecules formed at high coverages can efficiently transport H atoms across the surface of alumina, which would affect flourination of the surface and thus influence the etch rate. We studied in detail the mechanism of hydrogen transport for the case of 2 adsorbed HF, which indicated Grotthuss-like transport of a proton,[25] *i.e.* the net migration of charge in a hydrogen bonded liquid where individual protons switch positions but do not physically migrate.

Using the geometry M_A^2 in Fig. 7 as the starting point, we studied two pathways leading to the formation and desorption of H_2O molecules. We found that there are high energetic barriers ranging from +0.9 eV to +1.8 eV that inhibit the association of hydroxyl groups into adsorbed water. By contrast, the desorption energies of the thus-formed water molecules were found to range from +0.2 eV to +1.2 eV, which can be overcome in actual experimental conditions, leading to the formation of gaseous H_2O as etch by-product. Any OH that persists on the surface at the end of HF pulse, due to the high energetic barrier for H_2O formation and desorption, is likely to lead to the competing growth reaction (*i.e.* ALD) in the ligand exchange pulse, which is undesirable.

Conclusion

Theoretical insights on the HF pulse in the thermal atomic layer etch (ALE) of monoclinic alumina were provided using DFT calculations. Based on reaction energetics of the postulated reactions, qualitative evidence suggesting the self-limiting nature of the HF pulse was found. Following that, explicit slab calculations were conducted to study the adsorption of 1 to 26 HF molecules per cell on a monoclinic alumina surface. While a single HF molecule readily dissociated on adsorbing to the alumina surface, a hydrogen bonded network of mixed dissociated and intact HF molecules was observed at higher coverages. Evidence

from surface binding energies and dissociated HF coverages indicated that the dissociative chemisorption of HF is self-limiting, as required for ALE, rather than etching away the oxide continuously. Based on a saturated surface model, a theoretical maximum etch rate was computed to be -0.57±0.02 Å/cycle (-20.0±0.8 ng/(cm^2 cycle)), which amounted to the removal of 0.5 monolayer of material per cycle. Mechanisms for various surface chemical reactions such as hydrogen transport and formation of the etch by-product H_2O were studied and their activation barriers were computed. Hydrogen transport was identified as a favourable event, whereas the formation and desorption of H_2O molecules were hindered by substantial energetic barriers of at least 0.9 and 0.2 eV respectively.

Acknowledgement

We thank Lam Research Corporation for gift funding. We acknowledge access to the Science Foundation Ireland funded computing cluster at Tyndall.

Supporting Information Available

The following files are available free of charge.

- **Supporting Information.** Convergence test results, density of states and band structure of bulk θ-alumina, Equations of the computed properties, detailed ($\bar{2}$01) surface geometries, description of the M_Y^X notation, Bader charge analysis of dissociated HF on alumina surface, Desorption of AlF_3 and Al_2F_6.

References

(1) Puurunen, R. L. Surface Chemistry of Atomic Layer Deposition: A Case Study for the Trimethylaluminum/Water Process. *J. Appl. Phys.* **2005**, *97*, 121301.

(2) George, S. M. Atomic Layer Deposition: An Overview. *Chem. Rev.* **2010**, *110*, 111-113.

(3) Elliott, S. D. Atomic-Scale Simulation of ALD Chemistry. *Semicond. Sci. Technol.* **2012**, *27*, 074008.

(4) Carver, C. T.; Plombon, J. J.; Romero, P. E.; Suri, S.; Tronic, T. A.; Turkot Jr., R. B. Atomic Layer Etching: An Industry Perspective. *ECS J. Solid State Sci. Technol.* **2015**, *4*, N5005-N5009.

(5) Loubet, N.; Hook, T.; Montanini, P.; Yeung, C. W.; Kanakasabapathy, S.; Guillom, M.; Yamashita, T.; Zhang, J.; Miao, X.; Wang, J. et al. Stacked Nanosheet Gate-All-Around Transistor to Enable Scaling Beyond FinFET. *2017 Symp. VLSI Technol.* **2017**, T230-T231.

(6) Donnelly, V. M.; Kornblit, A. Plasma Etching: Yesterday, Today, and Tomorrow. *J. Vac. Sci. Technol. A* **2013**, *31*, 050825.

(7) Lee, C. G. N.; Kanarik, K. J.; Gottscho, R. A. The Grand Challenges of Plasma Etching: A Manufacturing Perspective. *J. Phys. D: Appl. Phys.* **2014**, *47*, 273001.

(8) Faraz, T.; Roozeboom, F.; Knoops, H. C. M.; Kessels, W. M. M. Atomic Layer Etching: What Can We Learn from Atomic Layer Deposition? *ECS J. Solid State Sci. Technol.* **2015**, *4*, N5023-N5032.

(9) George, S. M.; Lee, Y. Prospects for Thermal Atomic Layer Etching Using Sequential, Self-Limiting Fluorination and Ligand-Exchange Reactions. *ACS Nano* **2016**, *10*, 4889-4894.

(10) Lee, Y.; Huffman, C.; George, S. M. Selectivity in Thermal Atomic Layer Etching Using Sequential, Self Limiting Fluorination and Ligand-Exchange Reactions. *Chem. Mater.* **2016**, *28*, 7657-7665.

(11) Kanarik, K. J.; Tan, S.; Yang, W.; Kim, T.; Lill, T.; Kabansky, A.; Hudson, E. A.; Ohba, T.; Nojiri, K.; Yu, J. et al. Predicting Synergy in Atomic Layer Etching. *J. Vac. Sci. Technol. A* **2017**, *35*, 05C302.

(12) Athavale, S.; Economou, D. Molecular-Dynamics Simulation of Atomic layer Etching of Silicon. *J. Vac. Sci. Technol. A* **1995**, *13*, 966-971.

(13) Kanarik, K. J.; Lill, T.; Hudson, E. A.; Sriraman, S.; Tan, S.; Marks, J.; Vahedi, V.; Gottscho, R. A. Overview of Atomic Layer Etching in the Semiconductor Industry. *J. Vac. Sci. Technol. A* **2015**, *33*, 020802.

(14) Oehrlein, G. S.; Metzler, D.; Li, C. Atomic Layer Etching at the Tipping Point: An Overview. *ECS J. Solid State Sci. Technol.* **2015**, *4*, N5041-N5053.

(15) Lee, Y.; George, S. M. Atomic Layer Etching of Al2O3 Using Sequential, Self-Limiting Thermal Reactions with $Sn(acac)_2$ and Hydrogen Fluoride. *ACS Nano* **2015**, *9*, 2061-2070.

(16) Lee, Y.; DuMont, J. W.; George, S. M. Mechanism of Thermal Al_2O_3 Atomic Layer Etching Using Sequential Reactions with $Sn(acac)_2$ and HF. *Chem. Mater.* **2015**, *27*, 3648-3657.

(17) Lee, Y.; DuMont, J. W.; George, S. M. Atomic Layer Etching of HfO_2 Using Sequential, Self-Limiting Thermal Reactions with $Sn(acac)_2$ and HF. *ECS J. Solid State Sci. Technol.* **2015**, *4*, N5013-N5022.

(18) Johnson, N. R.; Sun, H.; Sharma, K.; George, S. M. Thermal Atomic Layer Etching of Crystalline Aluminum Nitride Using Sequential, Self-Limiting Hydrogen Fluoride and $Sn(acac)_2$ Reactions and Enhancement by H_2 and Ar Plasmas. *J. Vac. Sci. Technol. A* **2016**, *34*, 050603.

(19) Lee, Y.; DuMont, J. W.; George, S. M. Trimethylaluminum as the Metal Precursor for the Atomic Layer Etching of Al_2O_3 Using Sequential, Self-Limiting Thermal Reactions. *Chem. Mater.* **2016**, *28*, 2994-3003.

(20) Hennessy, J.; Moore, C. S.; Balasubramanian, K.; Jewell, A. D.; France, K.; Nikzad, S. Enhanced Atomic Layer Etching of Native Aluminum Oxide for Ultraviolet Optical Applications. *J. Vac. Sci. Technol. A* **2017**, *35*, 041512.

(21) DuMont, J. W.; George, S. M. Competition Between Al_2O_3 Atomic Layer Etching and AlF_3 Atomic Layer Deposition Using Sequential Exposures of Trimethylaluminum and Hydrogen Fluoride. *J. Chem. Phys.* **2017**, *146*, 052819.

(22) Henkelman, G.; Uberuaga, B. P.; Jonsson, H. A Climbing Image Nudged Elastic Band Method for Finding Saddle Points and Minimum Energy Paths. *J. Chem. Phys.* **2000**, *113*, 9901-9904.

(23) Henkelman, G.; Jonsson, H. Improved Tangent Estimate in the Nudged Elastic Band Method for Finding Minimum Energy Paths and Saddle Points. *J. Chem. Phys.* **2000**, *113*, 9978-9985.

(24) Quan, J.-L.; Teng, B.-T.; Wen, X.-D.; Zhao, Y.; Liu, R.; Luo, M.-F. Hydrogen Fluoride Adsorption and Reaction on the Alpha-Al_2O_3(0001) Surface: A Density Functional Theory Study. *J. Chem. Phys.* **2012**, *136*, 114701.

(25) Agmon, N. The Grotthuss Mechanism. *Chem. Phys. Lett.* **1995**, *244*, 456.

(26) Kresse, G.; Furthmuller, J. Efficient Iterative Schemes for Ab Initio Total-Energy Calculations Using a Plane-Wave Basis Set. *Phys. Rev. B* **1996**, *54*, 11169.

(27) Perdew, J. P.; Burke, K.; Ernzerhof, M. Generalized Gradient Approximation Made Simple. *Phys. Rev. Lett.* **1996**, *77*, 3865.

(28) Blochl, P. Projector Augmented-Wave Method. *Phys. Rev. B* **1994**, *50*, 17953.

(29) Kresse, G.; Joubert, D. From Ultrasoft Pseudopotentials to the Projector Augmented-Wave Method. *Phys. Rev. B* **1999**, *59*, 1758.

(30) Elliott, S. D.; Greer, J. C. Simulating the Atomic Layer Deposition of Alumina from First Principles. *J. Mater. Chem.* **2004**, *14*, 3246-3250.

(31) Broas, M.; Kanninen, O.; Vuorinen, V.; Tilli, M.; Paulasto-Krockel, M. Chemically Stable Atomic-Layer-Deposited Al_2O_3 Films for Processability. *ACS omega* **2017**, *2*, 3390-3398.

(32) Borosy, A.; Silvi, B.; Allavena, M.; Nortier, P. Structure and Bonding of Bulk and Surface Theta-Alumina from Periodic Hartree-Fock Calculations. *J. Phys. Chem.* **1994**, *98*, 13189-13194.

(33) Cai, S. H.; Rashkeev, S. N.; Pantelides, S. T.; Sohlberg, K. Atomic Scale Mechanism of the Transformation of Gamma-Alumina to Theta-Alumina. *Phys. Rev. Lett.* **2002**, *89*, 235501.

(34) Łodziana, Z.; Topsøe, N. Y.; Nørskov, J. K. A Negative Surface Energy for Alumina. *Nat. Mater.* **2004**, *3*, 289-293.

(35) Zhou, R.; Snyder, R. Structures and Transformation Mechanisms of the Eta, Gamma and Theta Transition Aluminas. *Acta Crystallogr. B* **1991**, *47*, 617-630.

(36) Henkelman, G.; Arnaldsson, A.; Jonsson, H. A fast and Robust Algorithm for Bader Decomposition of Charge Density. *Comput. Mater. Sci.* **2006**, *36*, 354-360.

(37) Tkatchenko, A.; Scheffler, M. Accurate Molecular Van Der Waals Interactions from Ground-State Electron Density and Free-Atom Reference Data. *Phys. Rev. Lett.* **2009**, *102*, 073005.

Table 1: Lattice parameters of monoclinic θ-Al_2O_3 computed with PBE XC functional with and without dispersion correction (TS - Tkatchenko-Scheffler method[37])are compared with experimental results.[35] A close agreement between the calculated and experimental values is observed, with a slight improvement due to inclusion of dispersion correction.

Lattice parameter	DFT (PBE)	DFT (PBE+TS)	Experiment[35]
a [Å]	11.94	11.85	11.85
b [Å]	2.94	2.92	2.90
c [Å]	5.67	5.63	5.62
α [°]	90.00	90.00	90.00
β [°]	103.99	104.01	103.83
γ [°]	90.00	90.00	90.00

Table 2: Reaction energies (ΔE) of postulated reactions of the HF pulse are compared for two scenarios, bulk $\longrightarrow$ gas (continuous etching) and surf $\longrightarrow$ surf (self-limiting) reactions. The energy values are normalized per unit Al_2O_3 and per HF molecule for comparison purposes. The ΔE values within parentheses refer to the PBE0 hybrid functional. (b) refers to bulk, (g) to gas-phase and (surf) to surface.

Label	Possible reactions	ΔE [eV/Al_2O_3]	ΔE [eV/HF]
	bulk $\longrightarrow$ gas		
R_1	$Al_2O_{3(b)} + 6\,HF_{(g)} \longrightarrow 2\,AlF_{3(g)} + 3\,H_2O_{(g)}$	0.40 (0.66)	0.07 (0.11)
R_2	$Al_2O_{3(b)} + 6\,HF_{(g)} \longrightarrow Al_2F_{6(g)} + 3\,H_2O_{(g)}$	-1.53 (-1.41)	-0.26 (-0.24)
R_3	$Al_2O_{3(b)} + 2\,HF_{(g)} \longrightarrow 2\,AlOF_{(g)} + H_2O_{(g)}$	9.88 (10.84)	4.94 (5.42)
	surf $\longrightarrow$ surf		
R_4	$3\,Al_2O_{3(surf)} + 18\,HF_{(g)} \longrightarrow 6\,AlF_{3(surf)} + 9\,H_2O_{(g)}$	-3.60	-0.60

Table 3: Adsorbate coverages and binding energies are tabulated for the minimum geometries M_Y^X given in Fig 7. Here, M_Y^X denotes a minimum with 'X' HF molecules and in case there are several minima they are indexed with a label 'Y'. HF coverage denotes the coverage of total number of HF molecules introduced in the supercell whereas Al-F coverage refers to the coverage of dissociated F atoms that form Al-F bonds.

Minima	HF coverage [/nm^2]	Al-F coverage [/nm^2]	E_{bind} [eV/HF]	E_{bind} [eV/nm^2]
M_A^2	1.2	1.2	-1.5	-1.8
M_B^2	1.2	0.6	-1.1	-1.3
M_C^2	1.2	0.6	-1.4	-1.7
M^3	1.8	0.6	-1.2	-2.0
M^5	3.0	0.6	-0.8	-2.5
M_A^8	4.8	4.8	-1.5	-7.1
M_B^8	4.8	2.4	-1.6	-7.6
M^{12}	7.1	3.6	-1.5	-10.5
M^{15}	8.9	4.8	-1.4	-12.1
M^{16}	9.5	9.5	-1.5	-13.9
M^{18}	10.7	4.8	-1.3	-13.7
M^{22}	13.1	4.8	-1.2	-15.1
M_A^{24}	14.3	9.5	-1.0	-14.4
M_B^{24}	14.3	13.7	-1.1	-16.2
M^{26}	15.5	7.1	-1.0	-16.0

Table 4: Activation energies for the barriers between minima involved in the H_2O formation pathways shown in Fig. 10. ΔE is the energy difference between the product (minimum) state and reactant (minimum) state

Barrier	Activation energy [eV]	ΔE [eV]
G1 $\longrightarrow$ G2	0.92	-0.14
G2 $\longrightarrow$ G1	1.06	0.14
G2 $\longrightarrow$ G3	1.63	1.21
G3 $\longrightarrow$ G2	0.19	-1.21
G2 $\longrightarrow$ G4	1.79	1.44
G4 $\longrightarrow$ G2	0.58	-1.44

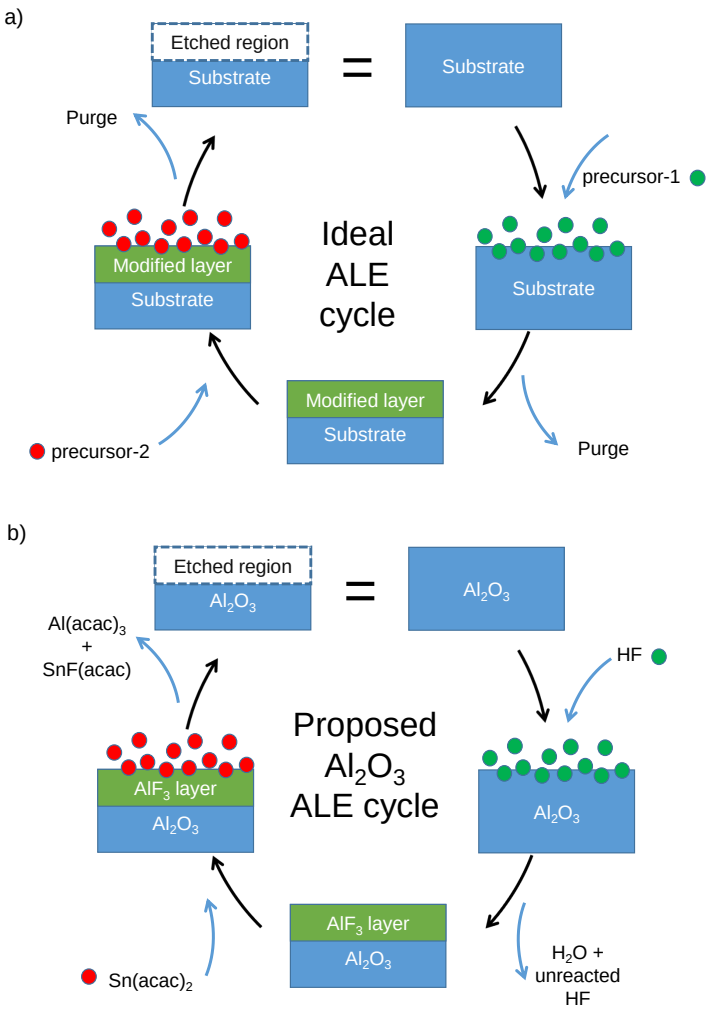

Figure 1: a) Schematic representation of an ideal ALE cycle. b) Schematic representation of a proposed Al_2O_3 ALE cycle.[15,16]

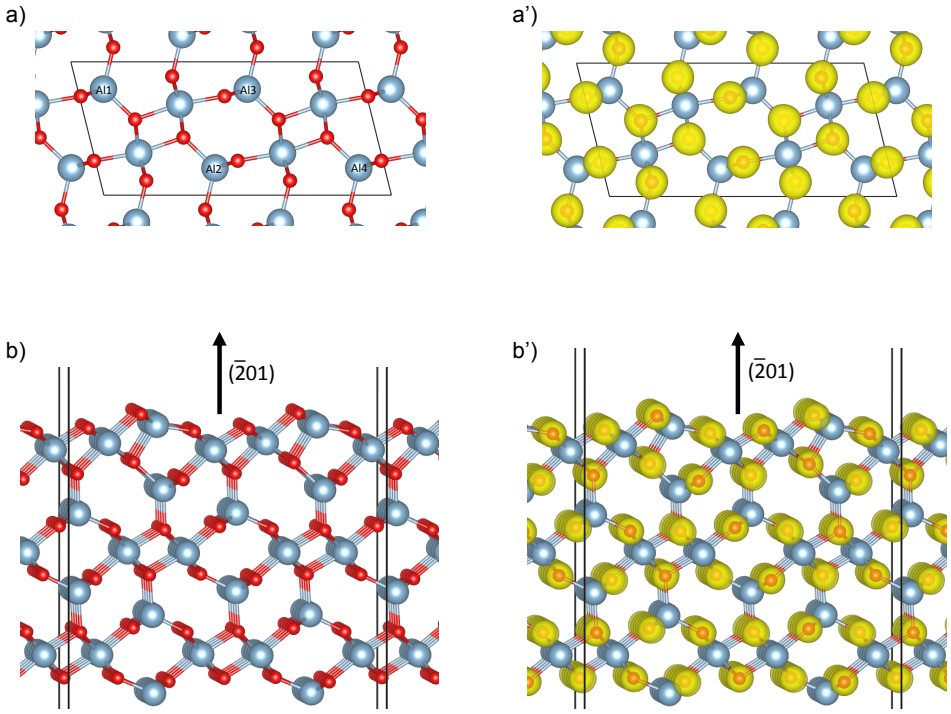

Figure 2: (a,a') The equilibrium geometry of bulk θ-Al_2O_3 along the *ac* lattice plane is shown in panel a and along with the valence charge density as yellow spheres in panel a'. The Al atoms marked with labels (Al1, Al2, Al3 and Al4) are found in tetrahedral coordination sites of the oxygen lattice, while those that are not marked are in octahedral coordination sites. The isosurface value is set to 0.2 e/Å^3. (b,b') The optimized geometry of $Al_2O_3(\bar{2}01)$ surface slab is shown in panel b and along with the valence charge density in panel b'. The isosurface value is set to 0.25 e/Å^3. It can be seen that the electrons are localized around the O atoms, which is an indication of predominantly ionic bonding between Al and O.

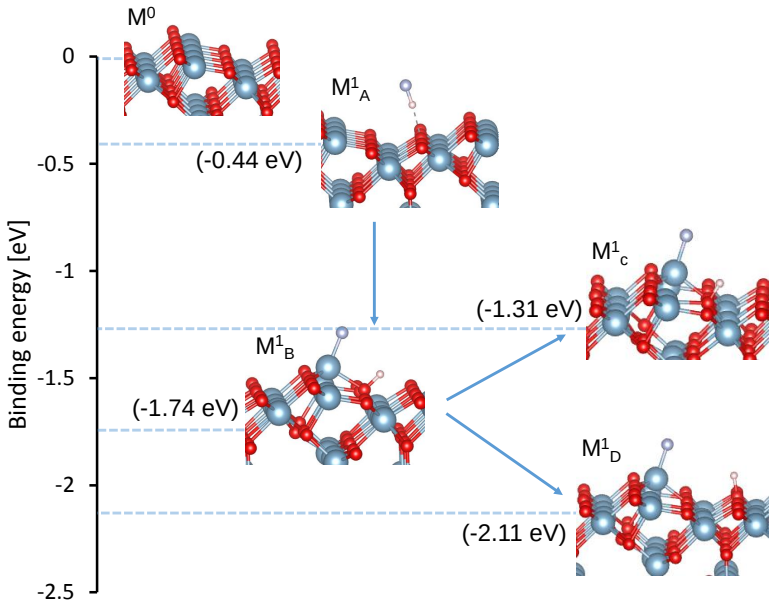

Figure 3: Chart showing the geometries and binding energies of identified minima with respect to 1 HF adsorption at θ-$Al_2O_3(\bar{2}01)$ surface. Here, M^0 corresponds to the clean alumina surface. M^1_A and M^1_B shows molecularly and dissociatively adsorbed HF, respectively. M^1_C and M^1_D refers to the geometries where the dissociated H atom hopped to an adjacent O atom in the same row and to an oxygen atom in the adjacent row, respectively. Activation energies where computed are shown in Fig 4.

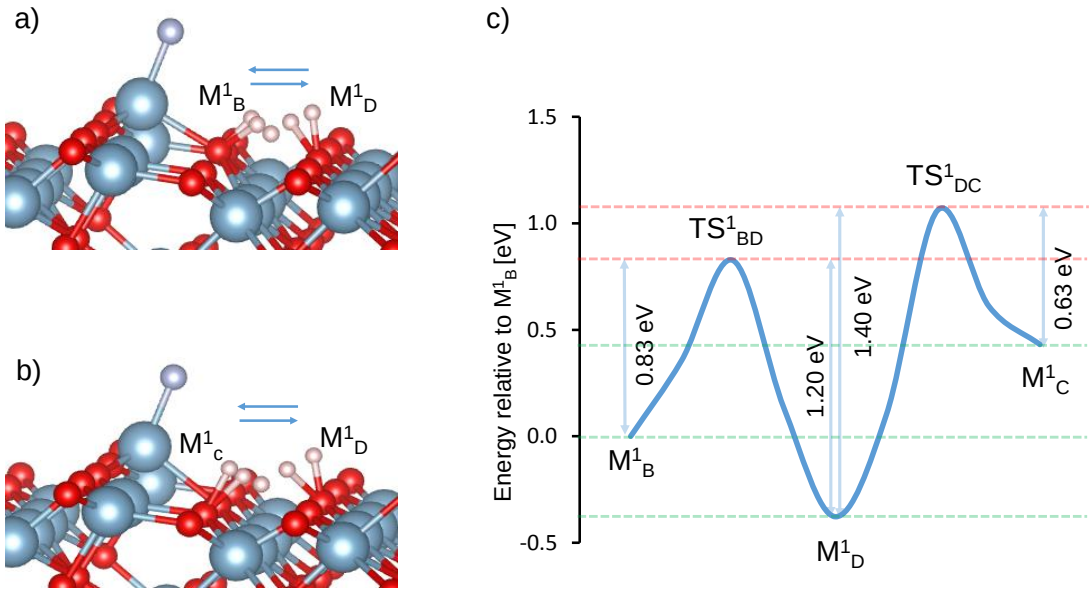

Figure 4: a) Pictorial representation of the pathway between minima M^1_B and M^1_D that shows an aggregate of all H atom positions as the H atom hops from one surface O atom to another O atom in the adjacent row. b) Similarly, for the pathway between minima M^1_D and M^1_C. Three images are chosen between the two minima and are optimized within CI-NEB approach. c) The graph shows the energy difference of the images with respect to M^1_B and the energy barriers with respect to a) and b). Here, TS^1_{BD} and TS^1_{DC} represent the transition states connecting M^1_B – M^1_D and M^1_D – M^1_C, respectively.

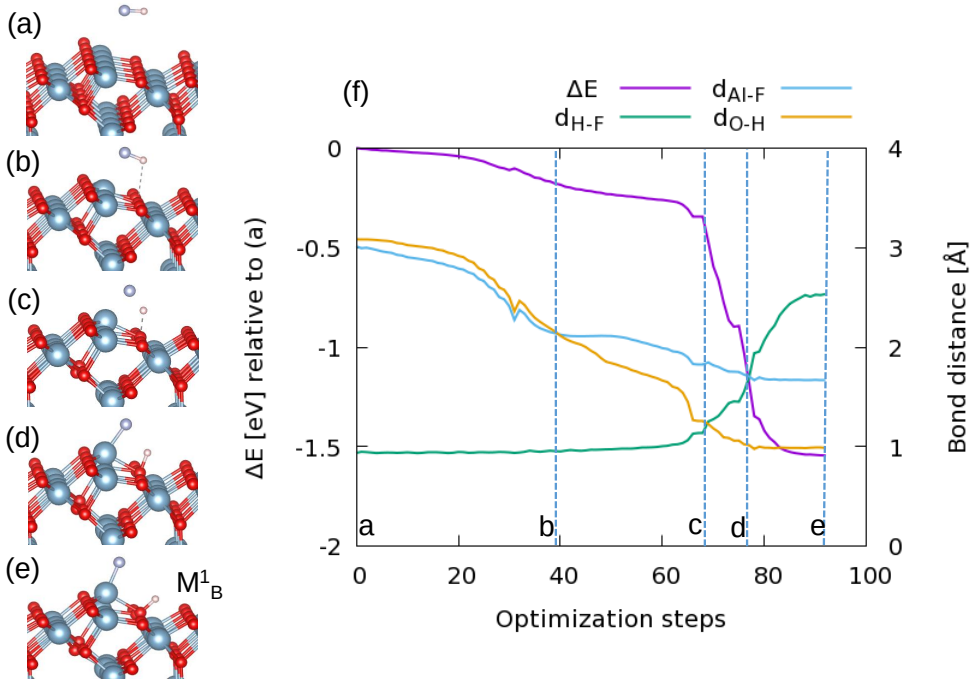

Figure 5: Spontaneous dissociative adsorption of HF molecule on θ-$Al_2O_3(\bar{2}01)$ surface. Snapshots taken from geometry optimization run where (a) is the chosen starting geometry with the HF molecule at least 3.0 Å from the surface. The HF molecule hydrogen bonds to a surface O atom in (b), the onset of the HF dissociation is given in (c), the completely dissociated HF forming -Al-F and -O-H species at the surface can be seen in (d) and the final optimized geometry M_B^1 in (e). The graph (f) shows the total energy of the system relative to the starting geometry (a) for the optimization steps along with the change in Al-F, H-F and O-H bond distances.

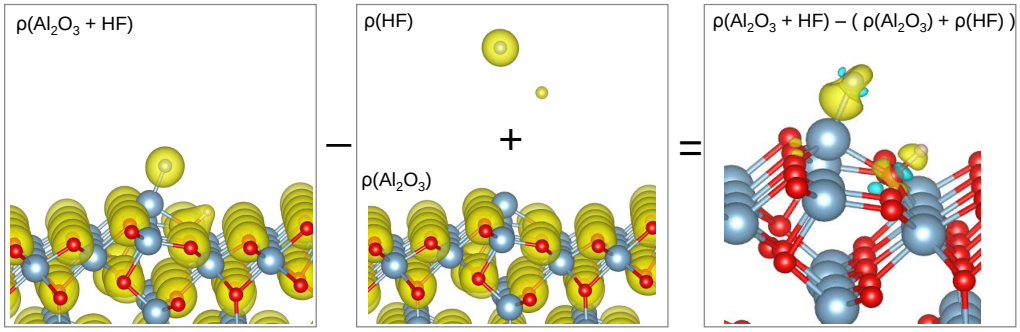

Figure 6: Analysis of charge density difference in geometry M_B^1. Here, the combined electronic charge density of the non-interacting systems ($\rho(Al_2O_3)$ and $\rho(HF)$) is subtracted from that of the interacting system ($\rho(Al_2O_3 + HF)$) to give the density difference plot in the right. The isosurface value for $\rho(Al_2O_3 + HF)$, $\rho(Al_2O_3)$ and $\rho(HF)$ is 0.1 e/Å^3. The isosurface value for the difference plot in the right is 0.02 e/Å^3.

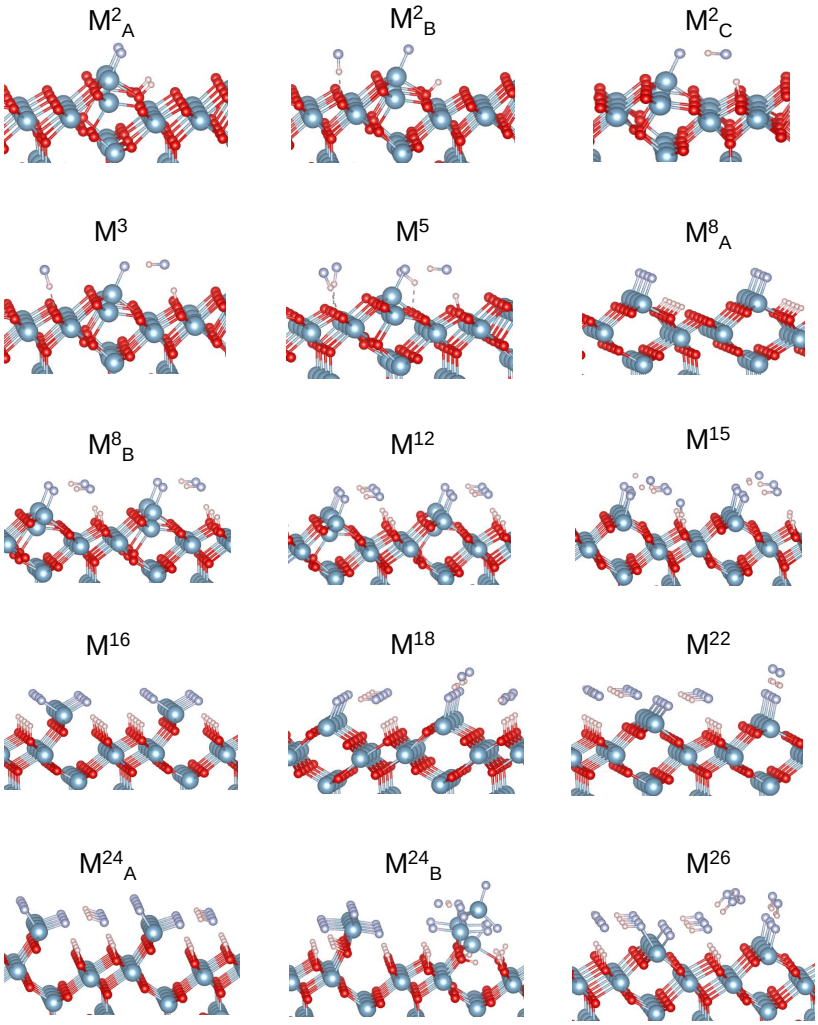

Figure 7: Optimized geometries of 2 - 26 HF molecules adsorbed on bare $Al_2O_3(\bar{2}01)$ surface. Here, M^X_Y denotes a minimum with 'X' HF molecules and in case there are several minima they are indexed with a label 'Y'. In some cases multiple minima are shown in order to convey the fact that very different stable configurations are possible. In most of the minimum geometries shown above, a mixed dissociative and molecular adsorption of HF molecules can be seen.

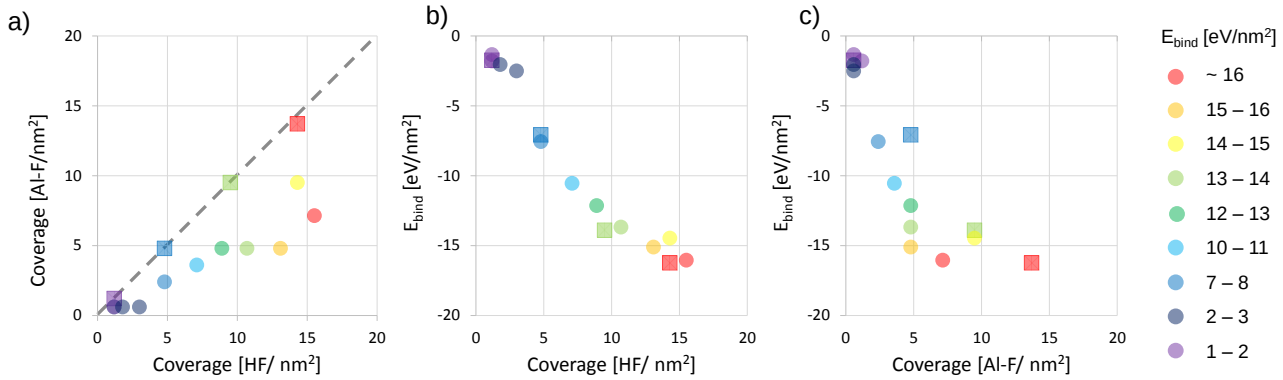

Figure 8: (a) A scatter plot showing the coverage of total HF adsorbed Vs the coverage of Al-F in the minima shown in Fig. 7. The data points are colored according to the corresponding total binding energy per nm^2 (color plot online). The square markers along the diagonal dashed line indicate geometries where the HF coverage is equal to Al-F coverage. Panels (b) and (c) show the change in binding energy per nm^2 with increase in HF and Al-F coverage, respectively.

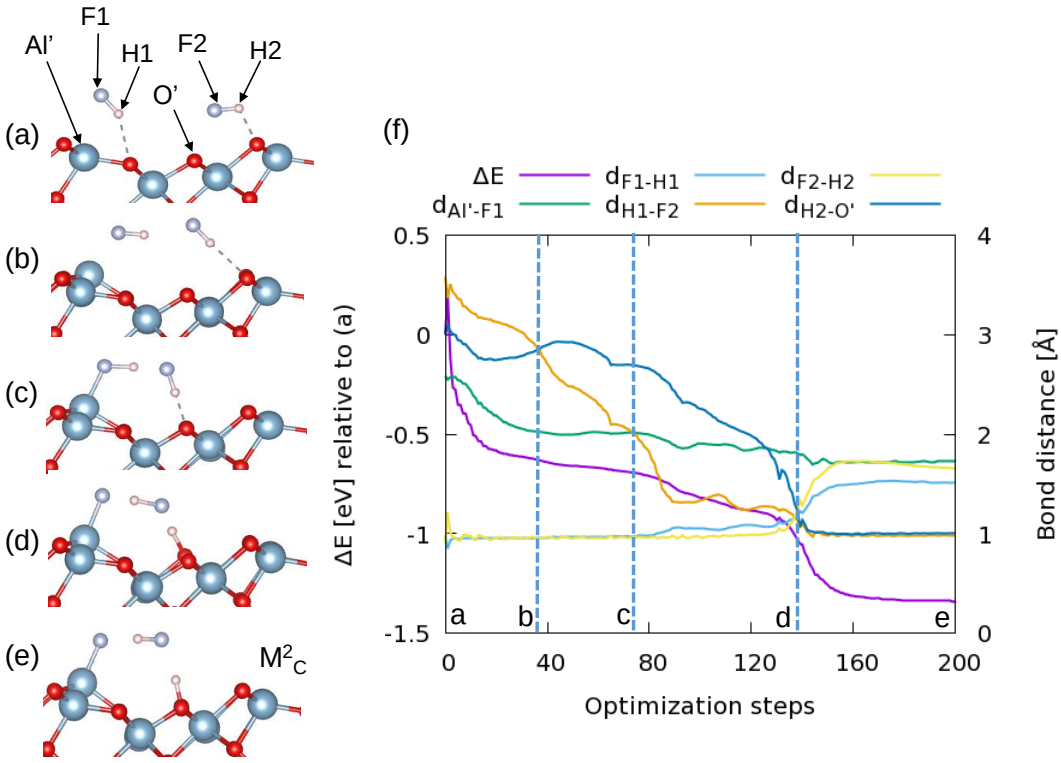

Figure 9: (a - e) Snapshots representing the hydrogen transport mechanism observed in the optimization of 2 HF molecules adsorbed on alumina surface to form M^2_C. (f) A complementary graph showing the trends of important inter-atomic distances and relative energy with respect to the initial geometry.

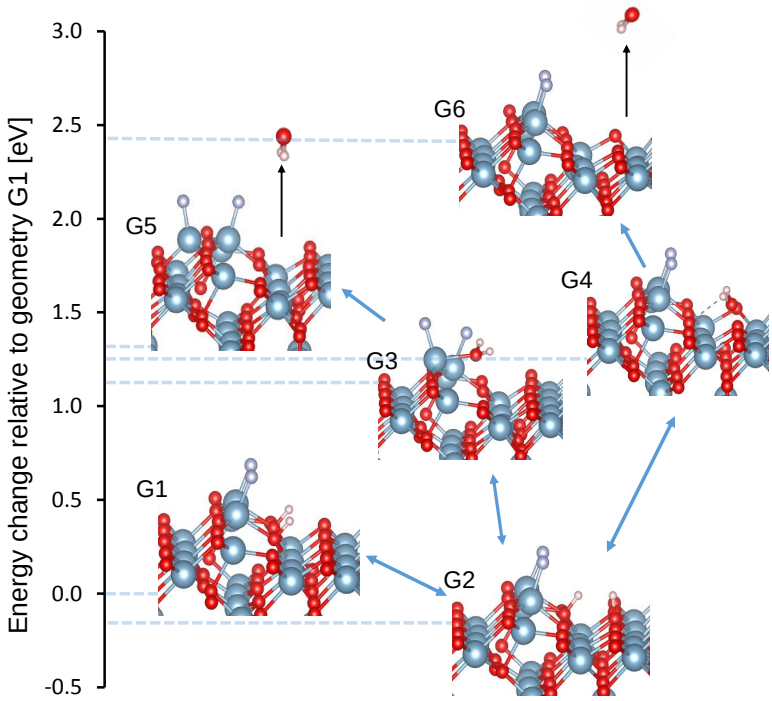

Figure 10: Pictorial representation of possible pathways in H_2O formation and desorption. The horizontal dotted line connecting each minimum corresponds to the energy change relative to geometry G1, which is also M_A^2 in Fig. 7

Graphical TOC Entry